Stability Assessment and Optimization of MMC Energy Balancing for Drive Applications at Standstill Using an Averaging Approach

Qiuye Gui[1,2] and Hendrik Fehr[1] and Albrecht Gensior[1]
[1]Technische Universität Ilmenau, Germany; [2]Technische Universität Dresden, Germany
qiuye.gui@tu-dresden.de; hendrik.fehr@tu-ilmenau.de; albrecht.gensior@tu-ilmenau.de

Acknowledgments

This work was supported by *Deutsche Forschungsgemeinschaft*, DFG, grant GE 2502/5-1. The test bench for the experiments has been provided by Chair of Power Electronics, Technische Universität Dresden.

Keywords

≪Converter control≫, ≪Modular Multilevel Converters (MMC)≫, ≪Non-linear control≫, ≪Optimization≫

Abstract

A new controller design framework for periodic systems is presented and applied to the Modular Multilevel Converter energy balancing. It provides a rigorous stability analysis for the state-of-art averaging control and the approach using constants as reference for the instantaneous energies. An optimized controller with improved performance is derived and verified by simulation and experiment.

Introduction

This paper focuses on the energy balancing issue of Modular Multilevel Converters (MMCs) with half-bridge cells in dc operation, i.e. a Permanent Magnet Synchronous Machine (PMSM) is fed at standstill, see Fig. 1. The balancing task is challenging due to the strong coupling [1, 2] and the underactuation of the energy model [3, 4]. The state-of-art approach [5–7] regulates the average value of equivalent arm voltages or stored arm energies by identifying current and voltage harmonic components that influence the respective average power terms. However, it does not provide a state-space model for the average energy which is derived mathematically from the circuit model. What's more, although the average values of the energies are controlled, no stability w.r.t. the energy ripples is confirmed, as an instability is possible due to the strong coupling effect. On the other hand, dynamic phasor models [8] and harmonic state-space approaches [9] describe the dynamics of all energy harmonics, but increase the system order

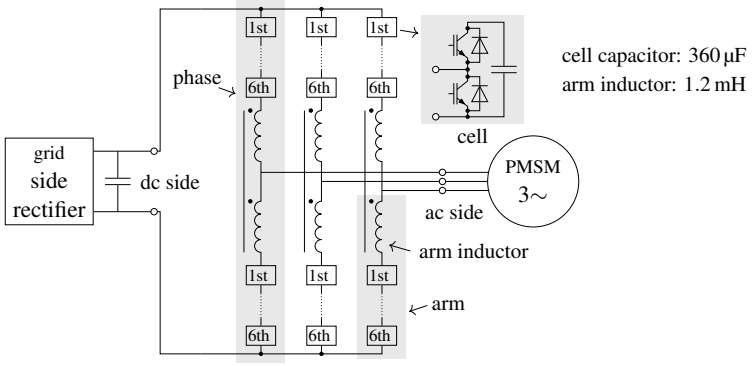

Fig. 1: Scheme of the application.

which makes them less attractive for model-based control design. To close the gap mentioned above, [3] provides an average energy model with mathematical background for a simple systematic model-based energy controller design. However, the model is based on a theorem from [10] which is limited to a finite time interval and thus cannot confirm stability of the proposed control system beyond that range. Moreover, the analysis in [3] focuses on the case which coincides with the average value control, and thus excludes approaches like [1] where a constant is used as reference for the instantaneous energies.

The present work provides a new controller design framework for periodic systems, and applies it to the energy controller design of an MMC. The framework extends the stability analysis in [3] to the whole time range $t \in [0,\infty)$. Compared with [9] which only provides a region of attraction in an uncertain small neighborhood of a stationary regime, it also provides a global stability assessment of the proposed control system. The energy reference can either be a stationary operating regime or a constant, which confirms the exponential convergence of average value controls like [5] and the stability of controls like [1] which use constants as reference for the instantaneous energies. Two controllers are derived: One with a simple choice of current harmonics and an optimized one leading to improved performance with two different common-mode voltage injections. Both results are verified by simulations and experiments.

A New Controller Design Framework Based on Averaging

In this section, the controller design problem for the state-space model[1]

$$\dot{\boldsymbol{x}} = \boldsymbol{f}_1(t,\boldsymbol{x},\boldsymbol{u}) \tag{1}$$

is considered, where the $n\times 1$ vector $\boldsymbol{x}$ and the $m\times 1$ vector $\boldsymbol{u}$ refer to the state and the input, respectively. Here, the task is to control the trajectory $t\mapsto \boldsymbol{x}(t)$ tracking its reference $t\mapsto \boldsymbol{x}_{\mathrm{ref}}(t)$ by means of $\boldsymbol{u}$ as the controller output with error dependency. With the error definition $\boldsymbol{x}_{\mathrm{err}} = \boldsymbol{x} - \boldsymbol{x}_{\mathrm{ref}}$, (1) can be rewritten as

$$\dot{\boldsymbol{x}}_{\mathrm{err}} = \boldsymbol{f}_1(t,\boldsymbol{x}_{\mathrm{err}} + \boldsymbol{x}_{\mathrm{ref}}(t), \boldsymbol{u}(\boldsymbol{x}_{\mathrm{err}})) - \dot{\boldsymbol{x}}_{\mathrm{ref}}(t) =: \boldsymbol{f}_2(t,\boldsymbol{x}_{\mathrm{err}},\boldsymbol{u}(\boldsymbol{x}_{\mathrm{err}}))\,. \tag{2}$$

If necessary, the integral of the error state can be easily introduced by means of regarding it as a part of the new error state. The next step should be the controller design, that is to specify an appropriate controller output $\boldsymbol{u}(\boldsymbol{x}_{\mathrm{err}})$ such that a desired dynamics or convergence of $\boldsymbol{x}_{\mathrm{err}}$ can be achieved. However, if the function $\boldsymbol{f}_2$ is nonlinear w.r.t. $\boldsymbol{x}_{\mathrm{err}}$ or $\boldsymbol{u}$, it may increase the controller design effort substantially. In the following, a new controller design framework is developed based on Theorem 10.4 in [11]. This framework deals with the case where the function $\boldsymbol{f}_2$ in (2) is periodic in t, and allows a simpler controller design, that is, the time dependency of $\boldsymbol{f}_2$ does not need to be considered during the controller design. First, the main results of Theorem 10.4 in [11] are recalled as follows:

Theorem 1 *Let $\boldsymbol{f}(\tau,\boldsymbol{x}_{\mathrm{err}},\boldsymbol{u}(\boldsymbol{x}_{\mathrm{err}}),\varepsilon)$ be an n-dimensional function with the following properties:*

(P1) The function itself and its partial derivatives w.r.t. $(\boldsymbol{x}_{\mathrm{err}},\varepsilon)$ up to the second order are continuous and bounded for $(\tau,\boldsymbol{x}_{\mathrm{err}},\varepsilon)\in[0,\infty)\times\mathbb{D}_1\times[0,\varepsilon_1]$, for some $\varepsilon_1>0$ and every compact set $\mathbb{D}_1\subset\mathbb{D}_2$, where $\mathbb{D}_2\subset\mathbb{R}^n$ is a domain containing the origin.

(P2) The function $\boldsymbol{f}$ is T-periodic in τ for some $T>0$, i.e. $\boldsymbol{f}(\tau+T,\boldsymbol{x}_{\mathrm{err}},\boldsymbol{u}(\boldsymbol{x}_{\mathrm{err}}),\varepsilon) = \boldsymbol{f}(\tau,\boldsymbol{x}_{\mathrm{err}},\boldsymbol{u}(\boldsymbol{x}_{\mathrm{err}}),\varepsilon)$, and has the average $\overline{\boldsymbol{f}}(\boldsymbol{x}_{\mathrm{err}},\boldsymbol{u}(\boldsymbol{x}_{\mathrm{err}}))$. It is obtained by averaging $\boldsymbol{f}$ w.r.t. τ at a vanishing ε and a τ-independent state $\boldsymbol{x}_{\mathrm{err}}$, i.e.

$$\overline{\boldsymbol{f}}(\boldsymbol{x}_{\mathrm{err}},\boldsymbol{u}(\boldsymbol{x}_{\mathrm{err}})) = \frac{1}{T}\int_0^T \boldsymbol{f}(\tau,\boldsymbol{x}_{\mathrm{err}},\boldsymbol{u}(\boldsymbol{x}_{\mathrm{err}}),0)\,\mathrm{d}\tau. \tag{3}$$

(P3) The solution $\tau\mapsto\boldsymbol{x}_{\mathrm{err}}(\tau)$ of the standard form of the original system

$$\frac{\mathrm{d}}{\mathrm{d}\tau}\boldsymbol{x}_{\mathrm{err}} = \varepsilon\boldsymbol{f}(\tau,\boldsymbol{x}_{\mathrm{err}},\boldsymbol{u}(\boldsymbol{x}_{\mathrm{err}}),\varepsilon) \tag{4}$$

[1] In this work, $\dot{x} := \mathrm{d}x/\mathrm{d}t$.

and the solution $\tau \mapsto \bar{\boldsymbol{x}}_{\mathrm{err}}(\tau)$ *of the standard form of the average system*

$$\frac{\mathrm{d}}{\mathrm{d}\tau}\bar{\boldsymbol{x}}_{\mathrm{err}} = \varepsilon \bar{\boldsymbol{f}}\left(\bar{\boldsymbol{x}}_{\mathrm{err}}, \boldsymbol{u}\left(\bar{\boldsymbol{x}}_{\mathrm{err}}\right)\right), \tag{5}$$

start at the same initial value, that is $\bar{\boldsymbol{x}}_{\mathrm{err}}(0) = \boldsymbol{x}_{\mathrm{err}}(0)$.

(P4) The origin $\bar{\boldsymbol{x}}_{\mathrm{err}} = \mathbf{0} \in \mathbb{D}_2$ *is an exponentially stable equilibrium point of* (5) *and* $\bar{\boldsymbol{x}}_{\mathrm{err}}(0) \in \mathbb{D}_3$ *where* $\mathbb{D}_3 \subset \mathbb{D}_2$ *is a compact subset of its region of attraction.*

Then there exists an $\varepsilon_2 > 0$ *such that for all* $0 < \varepsilon < \varepsilon_2$, $\|\boldsymbol{x}_{\mathrm{err}}(\tau) - \bar{\boldsymbol{x}}_{\mathrm{err}}(\tau)\| \leq c\varepsilon$ *(for some* $c > 0$*) is valid for all* $\tau \in [0, \infty)$*, and the origin of the original system* (4) *is exponentially stable if the following additional condition is satisfied:*

(P5) The function $\boldsymbol{f}\left(\tau, \boldsymbol{x}_{\mathrm{err}}, \boldsymbol{u}\left(\boldsymbol{x}_{\mathrm{err}}\right), \varepsilon\right)$ *satisfies* $\boldsymbol{f}\left(\tau, \mathbf{0}, \boldsymbol{u}\left(\mathbf{0}\right), \varepsilon\right) = \mathbf{0}$*, that is, the origin is an equilibrium point of the original system* (4)*.*

Here, the state of the average system is represented by $\bar{\boldsymbol{x}}_{\mathrm{err}}$ in order to distinguish from $\boldsymbol{x}_{\mathrm{err}}$ for the original system. Under the required conditions, this theorem confirms a stability of the original system (4), that is, it's solution always lies in a neighborhood of the solution of the average system (5) which converges exponentially to $\mathbf{0}$. Therefore, an alternative method for the state-space model based control system design can be provided. Instead of considering a complicated original system, the controller design can be accomplished at a simplified average system, derived by (3). This method can be summarized as the flow chart shown in Fig. 2.

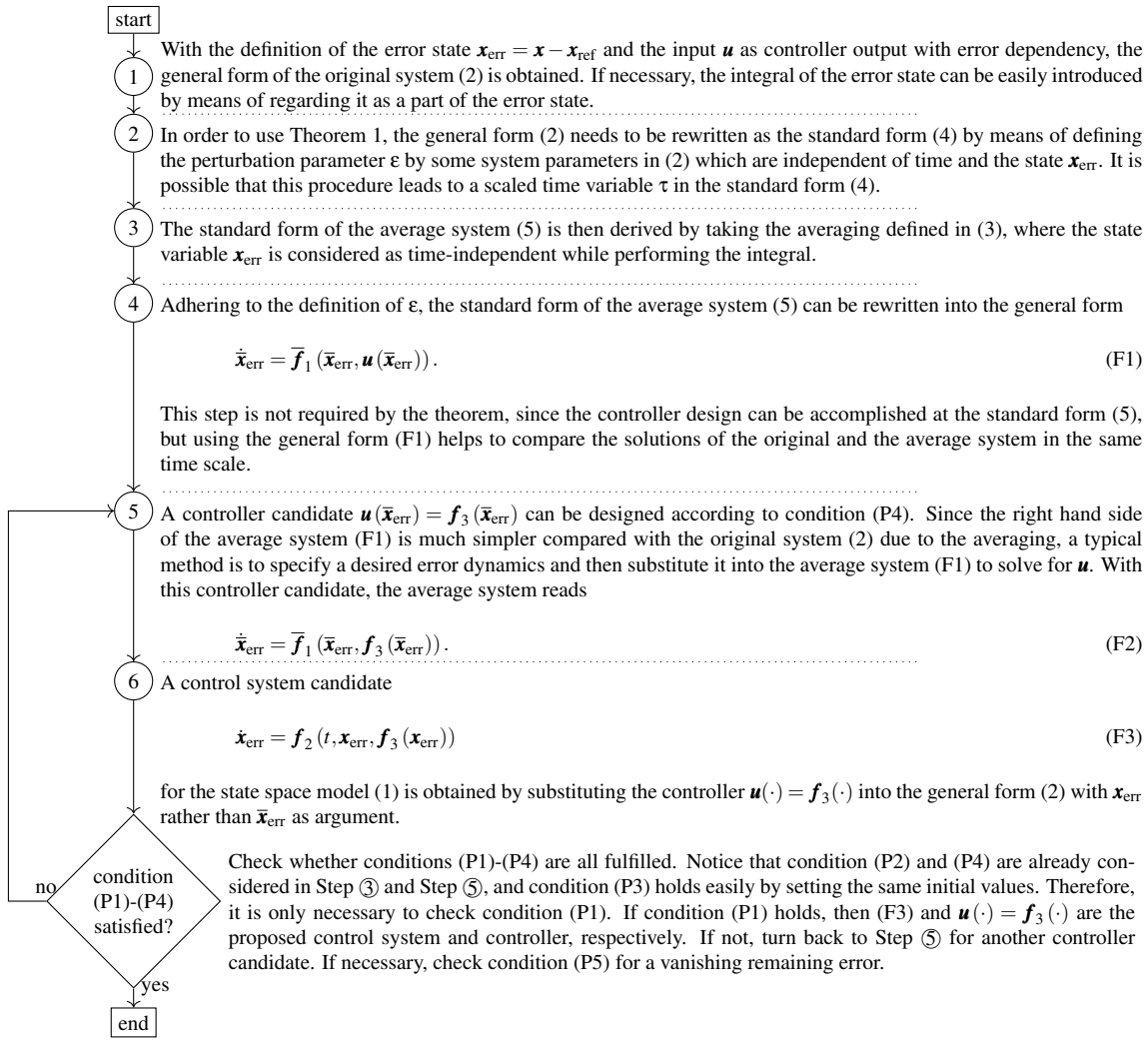

Fig. 2: Flow chart for the controller design framework based on Theorem 1.

Since the parameter ε is defined by some system parameters independent of time and state variable, it is expected that the solutions of a standard form and the corresponding general form are equivalent to each other in their individual time scales. Since the origin of the average system is exponentially stable, according to Theorem 1, with the designed controller and a sufficiently small ε, the solution $\boldsymbol{x}_{\mathrm{err}}(t)$ of the proposed control system (F3) converges to a neighborhood of $\mathbf{0}$ as $t \to \infty$, and the remaining error vanishes if the origin is an equilibrium point of the proposed control system (F3). This stability is for every initial value $\boldsymbol{x}_{\mathrm{err}}(0)$ lying in the region of attraction of the origin of the average system (F2).

Besides the conclusions, it is necessary to discuss the conditions required by Theorem 1. As for condition (P2), the function $\boldsymbol{f}(\tau, \boldsymbol{x}_{\mathrm{err}}, \boldsymbol{u}(\boldsymbol{x}_{\mathrm{err}}), \varepsilon)$ in (4) must be periodic in τ. Since the perturbation parameter ε is defined independent of t or $\boldsymbol{x}_{\mathrm{err}}$, a typical example is that the function $\boldsymbol{f}_1(t, \boldsymbol{x}_{\mathrm{err}} + \boldsymbol{x}_{\mathrm{ref}}(t), \boldsymbol{u}(\boldsymbol{x}_{\mathrm{err}}))$ and the reference $\boldsymbol{x}_{\mathrm{ref}}(t)$ in the system (2) are both periodic in t. The condition (P3) holds easily by setting the same initial values, while an appropriate controller design can ensure conditions (P1), (P4). This is expected to be accomplished without much effort since the controller design can be simplified after averaging. However, a challenge can be the choice of a sufficiently small ε. According to the analysis in [11], since ε_2 is generally difficult to calculate, a practical choice would be the definition of ε dependent on some parameters which can be changed by practical conditions or settings. In this way, it is possible that the parameter ε is able to approach a suitable value such that the proposed control system is stable.

Energy Model of Modular Multilevel Converters

In this text, a simplified energy model for MMCs as in [3] is considered:

$$\dot{e}_{s0} = v_{\mathrm{DC}} i_{s0} - \mathrm{Re}\left(\underline{v}_y^* \underline{i}\right) \qquad e_{s0}: \text{scaled total stored energy} \tag{6a}$$

$$\dot{e}_{d0} = -2 v_{y0} i_{s0} - \mathrm{Re}\left(\underline{i}_s^* \underline{v}_y\right) \qquad e_{d0}: \text{scaled total vertical energy difference} \tag{6b}$$

$$\dot{\underline{e}}_s = v_{\mathrm{DC}} \underline{i}_s - \underline{v}_y^* \underline{i}^* - 2\underline{i} v_{y0} \qquad \underline{e}_s: \text{complex energy sum} \tag{6c}$$

$$\dot{\underline{e}}_d = v_{\mathrm{DC}} \underline{i} - \underline{i}_s^* \underline{v}_y^* - 2\underline{i}_s v_{y0} - 2 i_{s0} \underline{v}_y \qquad \underline{e}_d: \text{complex energy difference.} \tag{6d}$$

The transformed energies can be summarized as $\boldsymbol{e} = \begin{pmatrix} e_{s0} & e_{d0} & \mathrm{Re}(\underline{e}_s) & \mathrm{Im}(\underline{e}_s) & \mathrm{Re}(\underline{e}_d) & \mathrm{Im}(\underline{e}_d) \end{pmatrix}^{\mathrm{T}}$. The currents i_{s0}, $\underline{i}_s$, and $\underline{i}$ denote the scaled dc current, the circulating current, and the complex ac-side current, respectively. The variables v_{DC}, v_{y0}, and $\underline{v}_y$ denote the dc-link voltage, the common-mode voltage, and the complex ac side voltage, respectively. Details of the variable definition and transformation can be found in [3]. Here, the current dynamics are neglected since they are much faster than the energy dynamics. Hence, in the dc operation, the ac-side current $\underline{i}$ and voltage $\underline{v}_y$ are considered to be constant. In order to realize the balancing task, harmonics w.r.t. a predetermined frequency ω_{cm} are injected in i_{s0}, $\underline{i}_s$, and v_{y0}. Therefore, the general form of injection reads

$$i_{s0} = I_{s0}^{[0]}(\boldsymbol{e}_{\mathrm{err}}, \boldsymbol{e}_{\mathrm{err,I}}) + \sum_{n \in \mathbb{Z}^+} \left(\underline{I}_{s0}^{[n]}(\boldsymbol{e}_{\mathrm{err}}, \boldsymbol{e}_{\mathrm{err,I}}) \mathrm{e}^{jn\omega_{\mathrm{cm}}t} + \underline{I}_{s0}^{[n]*}(\boldsymbol{e}_{\mathrm{err}}, \boldsymbol{e}_{\mathrm{err,I}}) \mathrm{e}^{-jn\omega_{\mathrm{cm}}t} \right) \tag{7a}$$

$$\underline{i}_s = \sum_{n \in \mathbb{Z}} \underline{I}_s^{[n]}(\boldsymbol{e}_{\mathrm{err}}, \boldsymbol{e}_{\mathrm{err,I}}) \mathrm{e}^{jn\omega_{\mathrm{cm}}t} \qquad \underline{i} = \underline{I}^{[0]} \qquad \underline{v}_y = \underline{V}_y^{[0]} \qquad v_{\mathrm{DC}} = V_{\mathrm{DC}}^{[0]} \tag{7b}$$

$$v_{y0} = \sum_{n \in \mathbb{N}_{\mathrm{cm}}} \left(\underline{V}_{y0}^{[n]} \mathrm{e}^{jn\omega_{\mathrm{cm}}t} + \underline{V}_{y0}^{[n]*} \mathrm{e}^{-jn\omega_{\mathrm{cm}}t} \right) \qquad \mathbb{N}_{\mathrm{cm}}: \text{made up of all harmonic orders of } v_{y0} \tag{7c}$$

where the coefficients $\underline{I}^{[0]}$, $\underline{V}_y^{[0]}$, $\underline{V}_{y0}^{[n]}$, and $V_{\mathrm{DC}}^{[0]}$ are constant, while the coefficients of i_{s0} and $\underline{i}_s$ might depend on the energy error $\boldsymbol{e}_{\mathrm{err}} = \boldsymbol{e} - \boldsymbol{e}_{\mathrm{ref}}$ and its integral $\boldsymbol{e}_{\mathrm{err,I}}$, obtained from $\dot{\boldsymbol{e}}_{\mathrm{err,I}} = \boldsymbol{e}_{\mathrm{err}}$, to facilitate the balancing task. This consideration covers the case where the coefficients are not constant due to the controller behavior. Two different common-mode voltage injections shown in Fig. 3 are considered. The coefficients for the red wave are given by (7c) with

$$n \in \mathbb{N}_{\mathrm{cm}} = \{1, 3\} \qquad \underline{V}_{y0}^{[1]} = 0.15 \cdot V_{\mathrm{DC}}^{[0]} \qquad \underline{V}_{y0}^{[3]} = -\left|\underline{V}_{y0}^{[1]}\right| / 6 \cdot \mathrm{e}^{j3\arg\left(\underline{V}_{y0}^{[1]}\right)} \tag{8}$$

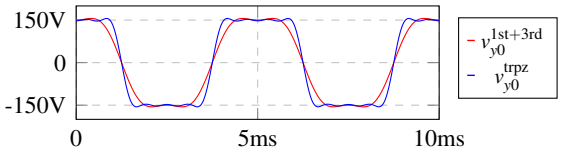

Fig. 3: Example of common-mode voltage: 1st+3rd harmonics $v_{y0}^{1st+3rd}$ (red, $\mathbb{N}_{cm}=\{1,3\}$, similar as [12] IV.B), approximated trapezoidal wave v_{y0}^{trpz} (blue, $\mathbb{N}_{cm}=\{1,3,5,7\}$).

where the third harmonic allows for an increased first harmonic $\underline{V}_{y0}^{[1]}$. The other wave in blue approximates a trapezoidal shape up to the 7th harmonic, given by (7c) with

$$n\in\mathbb{N}_{cm}=\{1,3,5,7\} \qquad \underline{V}_{y0}^{[n]}=\frac{V_{DC}^{[0]}}{4}\frac{\sin\left(n\frac{\pi}{2}\right)}{n\frac{\pi}{2}}\frac{\sin\left(n\frac{\pi}{10}\right)}{n\frac{\pi}{10}}. \tag{9}$$

In this text, the energy reference $\boldsymbol{e}_{ref}$, defined by $\dot{\boldsymbol{e}}_{ref}:=\boldsymbol{p}_{ref}(\omega_{cm}t)$, is either considered as a constant $\boldsymbol{E}$ with the derivative $\boldsymbol{p}_{ref}(\omega_{cm}t)=\boldsymbol{0}$, or a stationary operating regime $\boldsymbol{e}_{rgm}$, where $\boldsymbol{p}_{ref}(\omega_{cm}t)$ is $2\pi/\omega_{cm}$-periodic without drift. The calculation of the regimes will be discussed after the controller design.

Controller Design Based on the Proposed Framework

Step ①: Substituting the injection (7) into the energy model (6) leads to the system

$$\dot{\boldsymbol{e}}_{err}=\boldsymbol{p}_{dc}(\boldsymbol{e}_{err},\boldsymbol{e}_{err,I})+\boldsymbol{p}_{ac}(\omega_{cm}t,\boldsymbol{e}_{err},\boldsymbol{e}_{err,I})-\boldsymbol{p}_{ref}(\omega_{cm}t) \tag{10a}$$

$$\dot{\boldsymbol{e}}_{err,I}=\boldsymbol{e}_{err} \tag{10b}$$

with $\boldsymbol{p}_{dc}(\cdot,\cdot)=\begin{pmatrix} p_{dc,es0} & p_{dc,ed0} & \mathrm{Re}\left(\underline{p}_{dc,es}\right) & \mathrm{Im}\left(\underline{p}_{dc,es}\right) & \mathrm{Re}\left(\underline{p}_{dc,ed}\right) & \mathrm{Im}\left(\underline{p}_{dc,ed}\right)\end{pmatrix}^{T}$ and

$$p_{dc,es0}=V_{DC}^{[0]}I_{s0}^{[0]}(\boldsymbol{e}_{err},\boldsymbol{e}_{err,I})-\mathrm{Re}\left(\underline{V}_{y}^{[0]*}\underline{I}^{[0]}\right) \qquad \underline{p}_{dc,es}=V_{DC}^{[0]}\underline{I}_{s}^{[0]}(\boldsymbol{e}_{err},\boldsymbol{e}_{err,I})-\underline{V}_{y}^{[0]*}\underline{I}^{[0]*} \tag{11a}$$

$$p_{dc,ed0}=-\mathrm{Re}\left[4\sum_{n\in\mathbb{N}_{cm}}\underline{V}_{y0}^{[n]*}\underline{I}_{s0}^{[n]}(\boldsymbol{e}_{err},\boldsymbol{e}_{err,I})+\underline{V}_{y}^{[0]*}\underline{I}_{s}^{[0]}(\boldsymbol{e}_{err},\boldsymbol{e}_{err,I})\right] \tag{11b}$$

$$\begin{aligned}\underline{p}_{dc,ed}=&V_{DC}^{[0]}\underline{I}^{[0]}-\underline{V}_{y}^{[0]*}\underline{I}_{s}^{[0]*}(\boldsymbol{e}_{err},\boldsymbol{e}_{err,I})-2\underline{V}_{y}^{[0]}I_{s0}^{[0]}(\boldsymbol{e}_{err},\boldsymbol{e}_{err,I})\\&-2\sum_{n\in\mathbb{N}_{cm}}\left(\underline{V}_{y0}^{[n]}\underline{I}_{s}^{[-n]}(\boldsymbol{e}_{err},\boldsymbol{e}_{err,I})+\underline{V}_{y0}^{[n]*}\underline{I}_{s}^{[n]}(\boldsymbol{e}_{err},\boldsymbol{e}_{err,I})\right).\end{aligned} \tag{11c}$$

This corresponds to the general form (2), where $\boldsymbol{p}_{ac}$ and $\boldsymbol{p}_{dc}$ denote the power terms with and without explicit time dependency, respectively, while $\begin{pmatrix}\boldsymbol{e}_{err}^{T} & \boldsymbol{e}_{err,I}^{T}\end{pmatrix}^{T}$ represents the state variable. Here, function $\boldsymbol{p}_{ac}$ is $2\pi/\omega_{cm}$-periodic in t, that is $\boldsymbol{p}_{ac}(\omega_{cm}t,\boldsymbol{e}_{err},\boldsymbol{e}_{err,I})=\boldsymbol{p}_{ac}(\omega_{cm}(t+2\pi/\omega_{cm}),\boldsymbol{e}_{err},\boldsymbol{e}_{err,I})$.
Step ②: The perturbation parameter can be defined as $\varepsilon=1/\omega_{cm}$, which means that ε can be reduced by increasing the predetermined frequency ω_{cm}. By means of this definition, (10) can be rewritten as

$$\frac{\mathrm{d}}{\mathrm{d}\tau}\boldsymbol{e}_{err}=\varepsilon\left[\boldsymbol{p}_{dc}(\boldsymbol{e}_{err},\boldsymbol{e}_{err,I})+\boldsymbol{p}_{ac}(\tau,\boldsymbol{e}_{err},\boldsymbol{e}_{err,I})-\boldsymbol{p}_{ref}(\tau)\right] \qquad \frac{\mathrm{d}}{\mathrm{d}\tau}\boldsymbol{e}_{err,I}=\varepsilon\boldsymbol{e}_{err} \tag{12}$$

with the new time scale $\tau=\omega_{cm}t$. The term $\boldsymbol{p}_{ref}(\tau)$ is assumed to be explicitly independent of ε after the change of time scale, as will be confirmed in Step ⑥.
Step ③: As discussed at the end of the previous section, the term $\boldsymbol{p}_{ref}(\tau)$ is 2π-periodic in τ without drift. According to (3), the averaging of the right hand side of (12) reads

$$\frac{1}{2\pi}\int_{0}^{2\pi}\left[\boldsymbol{p}_{dc}(\boldsymbol{e}_{err},\boldsymbol{e}_{err,I})+\boldsymbol{p}_{ac}(\tau,\boldsymbol{e}_{err},\boldsymbol{e}_{err,I})-\boldsymbol{p}_{ref}(\tau)\right]\mathrm{d}\tau=\boldsymbol{p}_{dc}(\boldsymbol{e}_{err},\boldsymbol{e}_{err,I}) \tag{13a}$$

$$\frac{1}{2\pi}\int_0^{2\pi} \boldsymbol{e}_{\mathrm{err}}\mathrm{d}\tau = \boldsymbol{e}_{\mathrm{err}}. \tag{13b}$$

Notice that the states $\boldsymbol{e}_{\mathrm{err}}$ and $\boldsymbol{e}_{\mathrm{err,I}}$ are considered as time-independent while performing the integral. As a result, the average system

$$\frac{\mathrm{d}}{\mathrm{d}\tau}\overline{\boldsymbol{e}}_{\mathrm{err}} = \varepsilon \boldsymbol{p}_{\mathrm{dc}}\left(\overline{\boldsymbol{e}}_{\mathrm{err}}, \overline{\boldsymbol{e}}_{\mathrm{err,I}}\right) \qquad \frac{\mathrm{d}}{\mathrm{d}\tau}\overline{\boldsymbol{e}}_{\mathrm{err,I}} = \varepsilon \overline{\boldsymbol{e}}_{\mathrm{err}} \tag{14}$$

is obtained which corresponds to the standard form (5) in the framework. Here, the state is represented by $\begin{pmatrix} \overline{\boldsymbol{e}}_{\mathrm{err}}^{\mathrm{T}} & \overline{\boldsymbol{e}}_{\mathrm{err,I}}^{\mathrm{T}} \end{pmatrix}^{\mathrm{T}}$ in order to distinguish from $\begin{pmatrix} \boldsymbol{e}_{\mathrm{err}}^{\mathrm{T}} & \boldsymbol{e}_{\mathrm{err,I}}^{\mathrm{T}} \end{pmatrix}^{\mathrm{T}}$ for the original system.
Step ④: With the same definition $\varepsilon = 1/\omega_{\mathrm{cm}}$, system (14) can be rewritten as

$$\dot{\overline{\boldsymbol{e}}}_{\mathrm{err}} = \boldsymbol{p}_{\mathrm{dc}}\left(\overline{\boldsymbol{e}}_{\mathrm{err}}, \overline{\boldsymbol{e}}_{\mathrm{err,I}}\right) \qquad \dot{\overline{\boldsymbol{e}}}_{\mathrm{err,I}} = \overline{\boldsymbol{e}}_{\mathrm{err}} \tag{15}$$

which corresponds to the general form (F1) in the framework.
Step ⑤: For the system (15), the linear error dynamics

$$\dot{\overline{\boldsymbol{e}}}_{\mathrm{err}} = -k_{\mathrm{P,e}}\overline{\boldsymbol{e}}_{\mathrm{err}} - k_{\mathrm{I,e}}\overline{\boldsymbol{e}}_{\mathrm{err,I}} \qquad \dot{\overline{\boldsymbol{e}}}_{\mathrm{err,I}} = \overline{\boldsymbol{e}}_{\mathrm{err}} \tag{16}$$

is specified. This guarantees that the origin is globally exponentially stable if $k_{\mathrm{P,e}} > 0$, $k_{\mathrm{I,e}} > 0$. In this text, we choose $k_{\mathrm{I,e}} = k_{\mathrm{P,e}}^2/2$ in order to keep a good compromise between the rapidity and the overshoot of the solution of (16) [13]. Substituting the error dynamics (16) into the average system (15) leads to

$$-k_{\mathrm{P,e}}\overline{e}_{s0,\mathrm{err}} - k_{\mathrm{I,e}}\overline{e}_{s0,\mathrm{err,I}} = V_{\mathrm{DC}}^{[0]} I_{s0}^{[0]}\left(\overline{\boldsymbol{e}}_{\mathrm{err}}, \overline{\boldsymbol{e}}_{\mathrm{err,I}}\right) - \mathrm{Re}\left(\underline{V}_y^{[0]*}\underline{I}^{[0]}\right) \tag{17a}$$

$$-k_{\mathrm{P,e}}\underline{\overline{e}}_{s,\mathrm{err}} - k_{\mathrm{I,e}}\underline{\overline{e}}_{s,\mathrm{err,I}} = V_{\mathrm{DC}}^{[0]}\underline{I}_s^{[0]}\left(\overline{\boldsymbol{e}}_{\mathrm{err}}, \overline{\boldsymbol{e}}_{\mathrm{err,I}}\right) - \underline{V}_y^{[0]*}\underline{I}^{[0]*} \tag{17b}$$

$$-k_{\mathrm{P,e}}\overline{e}_{d0,\mathrm{err}} - k_{\mathrm{I,e}}\overline{e}_{d0,\mathrm{err,I}} = -\mathrm{Re}\left[4\sum_{n\in\mathbb{N}_{\mathrm{cm}}} \underline{V}_{y0}^{[n]*} I_{s0}^{[n]}\left(\overline{\boldsymbol{e}}_{\mathrm{err}}, \overline{\boldsymbol{e}}_{\mathrm{err,I}}\right) + \underline{V}_y^{[0]*}\underline{I}_s^{[0]}\left(\overline{\boldsymbol{e}}_{\mathrm{err}}, \overline{\boldsymbol{e}}_{\mathrm{err,I}}\right)\right] \tag{17c}$$

$$\begin{aligned} -k_{\mathrm{P,e}}\underline{\overline{e}}_{d,\mathrm{err}} - k_{\mathrm{I,e}}\underline{\overline{e}}_{d,\mathrm{err,I}} = {} & V_{\mathrm{DC}}^{[0]}\underline{I}^{[0]} - \underline{V}_y^{[0]*}\underline{I}_s^{[0]*}\left(\overline{\boldsymbol{e}}_{\mathrm{err}}, \overline{\boldsymbol{e}}_{\mathrm{err,I}}\right) - 2\underline{V}_y^{[0]} I_{s0}^{[0]}\left(\overline{\boldsymbol{e}}_{\mathrm{err}}, \overline{\boldsymbol{e}}_{\mathrm{err,I}}\right) \\ & - 2\sum_{n\in\mathbb{N}_{\mathrm{cm}}}\left(\underline{V}_{y0}^{[n]}\underline{I}_s^{[-n]}\left(\overline{\boldsymbol{e}}_{\mathrm{err}}, \overline{\boldsymbol{e}}_{\mathrm{err,I}}\right) + \underline{V}_{y0}^{[n]*}\underline{I}_s^{[n]}\left(\overline{\boldsymbol{e}}_{\mathrm{err}}, \overline{\boldsymbol{e}}_{\mathrm{err,I}}\right)\right). \end{aligned} \tag{17d}$$

Similar as the idea in [14, 15], the constant coefficients of the common-mode voltage avoid nonlinearities w.r.t. the candidates of the controller output in (17) such that the design effort can be reduced greatly. In the subsystem (17a) and (17b), only the coefficients $I_{s0}^{[0]}$ and $\underline{I}_s^{[0]}$ are available to accomplish the dynamics of $\overline{e}_{s0,\mathrm{err}}$ and $\underline{\overline{e}}_{s,\mathrm{err}}$, respectively. The corresponding solutions are

$$I_{s0}^{[0]}(\cdot,\cdot) = \left(-k_{\mathrm{P,e}}\overline{e}_{s0,\mathrm{err}} - k_{\mathrm{I,e}}\overline{e}_{s0,\mathrm{err,I}} + \mathrm{Re}\left(\underline{V}_y^{[0]*}\underline{I}^{[0]}\right)\right)/V_{\mathrm{DC}}^{[0]} \tag{18a}$$

$$\underline{I}_s^{[0]}(\cdot,\cdot) = \left(-k_{\mathrm{P,e}}\underline{\overline{e}}_{s,\mathrm{err}} - k_{\mathrm{I,e}}\underline{\overline{e}}_{s,\mathrm{err,I}} + \underline{V}_y^{[0]*}\underline{I}^{[0]*}\right)/V_{\mathrm{DC}}^{[0]}. \tag{18b}$$

However, from the subsystems (17c) and (17d), it is obvious that more than one current coefficient can be used for the dynamics of $\overline{e}_{d0,\mathrm{err}}$ and $\underline{\overline{e}}_{d,\mathrm{err}}$, respectively. In other words, the subsystem (17c) and (17d) is underdetermined and thus has infinite solutions. In the following, two solutions are derived, leading to two energy controllers:

• **simple choice**: Only one current coefficient is used for the dynamics of $\overline{e}_{d0,\mathrm{err}}$ or $\underline{\overline{e}}_{d,\mathrm{err}}$, respectively:

$$\underline{I}_{s0}^{[1]}(\cdot,\cdot) = \left(k_{\mathrm{P,e}}\overline{e}_{d0,\mathrm{err}} + k_{\mathrm{I,e}}\overline{e}_{d0,\mathrm{err,I}} - \mathrm{Re}\left(\underline{V}_y^{[0]*}\underline{I}_s^{[0]}(\cdot,\cdot)\right)\right) / \left(4\underline{V}_{y0}^{[1]*}\right) \tag{19a}$$

$$\underline{I}_s^{[1]}(\cdot,\cdot) = \left(k_{\mathrm{P,e}}\underline{\overline{e}}_{d,\mathrm{err}} + k_{\mathrm{I,e}}\underline{\overline{e}}_{d,\mathrm{err,I}} + V_{\mathrm{DC}}^{[0]}\underline{I}^{[0]} - \underline{V}_y^{[0]*}\underline{I}_s^{[0]*}(\cdot,\cdot) - 2\underline{V}_y^{[0]} I_{s0}^{[0]}(\cdot,\cdot)\right) / \left(2\underline{V}_{y0}^{[1]*}\right) \tag{19b}$$

Therefore, the whole controller is given by (18) and (19). It is very similar to the choice for lf-mode

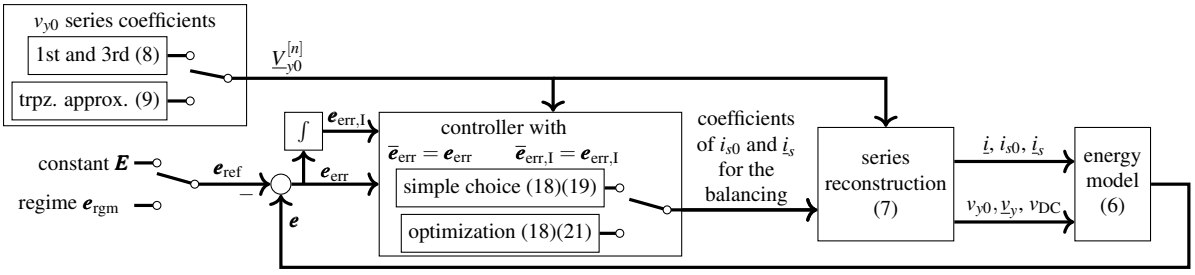

Fig. 4: Block diagram of the energy control system for the dc operation.

in [5] except for the usage of harmonics of order -1 in the complex circulating current. For this variant, the common-mode voltage is given by $v_{y0}^{\mathrm{1st+3rd}}$ as the red wave in Fig. 3.

• **optimization** for arm current Root Mean Square (RMS): This variant is derived by a quadratic programming problem with linear constraints. The objective function is given by

$$f_{\mathrm{obj}} = 4 \sum_{n\in\mathbb{N}_{\mathrm{cm}}} \left|\underline{I}_{s0}^{[n]}(\cdot,\cdot)\right|^2 + \sum_{n\in\mathbb{N}_{\mathrm{cm}}} \left(\left|\underline{I}_{s}^{[n]}(\cdot,\cdot)\right|^2 + \left|\underline{I}_{s}^{[-n]}(\cdot,\cdot)\right|^2 \right) \tag{20}$$

and it is subjected to (17c) and (17d). According to the variable definition given in [3], since the ac-side current $\underline{i} = \underline{I}^{[0]}$ is fixed by the load, and $I_{s0}^{[0]}(\cdot,\cdot)$ and $\underline{I}_{s}^{[0]}(\cdot,\cdot)$ are fixed by (17a) and (17b), respectively, the minimum of (20) leads to the minimal arm current RMS if the MMC enters a stationary regime where all current coefficients are constant. This optimization problem is convex, and the result leads to the optimized controller given by (18) and

$$\underline{I}_{s0}^{[n]}(\cdot,\cdot) = \underline{V}_{y0}^{[n]} \left(k_{\mathrm{P,ed0}} \bar{e}_{d0,\mathrm{err}} + k_{\mathrm{I,ed0}} \bar{e}_{d0,\mathrm{err,I}} - \mathrm{Re}\left(\underline{V}_{y}^{[0]} \underline{I}_{s}^{[0]*}(\cdot,\cdot) \right) \right) / (4S) \tag{21a}$$

$$\underline{I}_{s}^{[-n]}(\cdot,\cdot) = \underline{V}_{y0}^{[n]*} \left(k_{\mathrm{P,ed}} \underline{\bar{e}}_{d,\mathrm{err}} + k_{\mathrm{I,ed}} \underline{\bar{e}}_{d,\mathrm{err,I}} + V_{\mathrm{DC}}^{[0]} \underline{I}^{[0]} - \underline{V}_{y}^{[0]*} \underline{I}_{s}^{[0]*}(\cdot,\cdot) - 2\underline{V}_{y}^{[0]} I_{s0}^{[0]}(\cdot,\cdot) \right) / (4S) \tag{21b}$$

$$\underline{I}_{s}^{[n]}(\cdot,\cdot) = \underline{V}_{y0}^{[n]} \left(k_{\mathrm{P,ed}} \underline{\bar{e}}_{d,\mathrm{err}} + k_{\mathrm{I,ed}} \underline{\bar{e}}_{d,\mathrm{err,I}} + V_{\mathrm{DC}}^{[0]} \underline{I}^{[0]} - \underline{V}_{y}^{[0]*} \underline{I}_{s}^{[0]*}(\cdot,\cdot) - 2\underline{V}_{y}^{[0]} I_{s0}^{[0]}(\cdot,\cdot) \right) / (4S) \tag{21c}$$

with $n \in \mathbb{N}_{\mathrm{cm}}$ and $S = \sum_{m\in\mathbb{N}_{\mathrm{cm}}} |\underline{V}_{y0}^{[m]}|^2$. This controller enables all feasible current harmonics for the subsystem (17c) and (17d). For this controller, the common-mode voltage can be given by either $v_{y0}^{\mathrm{1st+3rd}}$ or v_{y0}^{trpz} in Fig. 3.

Step ⑥: Using the designed controller with the substitution $\bar{\boldsymbol{e}}_{\mathrm{err}} = \boldsymbol{e}_{\mathrm{err}}$ and $\bar{\boldsymbol{e}}_{\mathrm{err,I}} = \boldsymbol{e}_{\mathrm{err,I}}$, the energy control system in Fig. 4 is derived. Regarding the stationary operating regime $\boldsymbol{e}_{\mathrm{rgm}}$, it can be designed such that condition (P5) is fulfilled. In this case, the origin becomes an equilibrium point of the system which, by (P5), ensures a vanishing remaining energy error. This leads to $\boldsymbol{p}_{\mathrm{ref}}(\omega_{\mathrm{cm}} t) = \boldsymbol{p}_{\mathrm{dc}}(\boldsymbol{0},\boldsymbol{0}) + \boldsymbol{p}_{\mathrm{ac}}(\omega_{\mathrm{cm}} t, \boldsymbol{0}, \boldsymbol{0})$ which is derived from (10) with $\boldsymbol{e}_{\mathrm{err}} = \boldsymbol{0}$ and $\boldsymbol{e}_{\mathrm{err,I}} = \boldsymbol{0}$. In other words, a feasible stationary operating regime can be obtained by integrating the energy model (6) analytically, where the corresponding current injection is determined by the energy controller with vanishing energy error, and the average value of the regime is set to the constant $\boldsymbol{E}$. With the designed controller and the regime discussed above, it is obvious that all conditions in Theorem 1 hold, and the system in Fig. 4 is the proposed energy control system for dc operation.

According to Theorem 1, for a sufficiently large frequency ω_{cm} and with the same initial values, the error $\left(\begin{array}{cc} \boldsymbol{e}_{\mathrm{err}}^{\mathrm{T}}(t) & \boldsymbol{e}_{\mathrm{err,I}}^{\mathrm{T}}(t) \end{array} \right)^{\mathrm{T}}$ of the proposed energy control system lies in a neighborhood of the solution $\left(\begin{array}{cc} \bar{\boldsymbol{e}}_{\mathrm{err}}^{\mathrm{T}}(t) & \bar{\boldsymbol{e}}_{\mathrm{err,I}}^{\mathrm{T}}(t) \end{array} \right)^{\mathrm{T}}$ of the corresponding average system (16) which converges globally and exponentially to $\boldsymbol{0}$, and the remaining error vanishes when the energy reference is given by the regime $\boldsymbol{e}_{\mathrm{rgm}}$. This is confirmed by the simulations in Fig. 5. In other words, for a sufficiently large predetermined frequency ω_{cm}, the MMC energy $\boldsymbol{e}(t)$ converges globally to a neighborhood of the constant reference $\boldsymbol{E}$, or it tracks the calculated regime $\boldsymbol{e}_{\mathrm{rgm}}$.

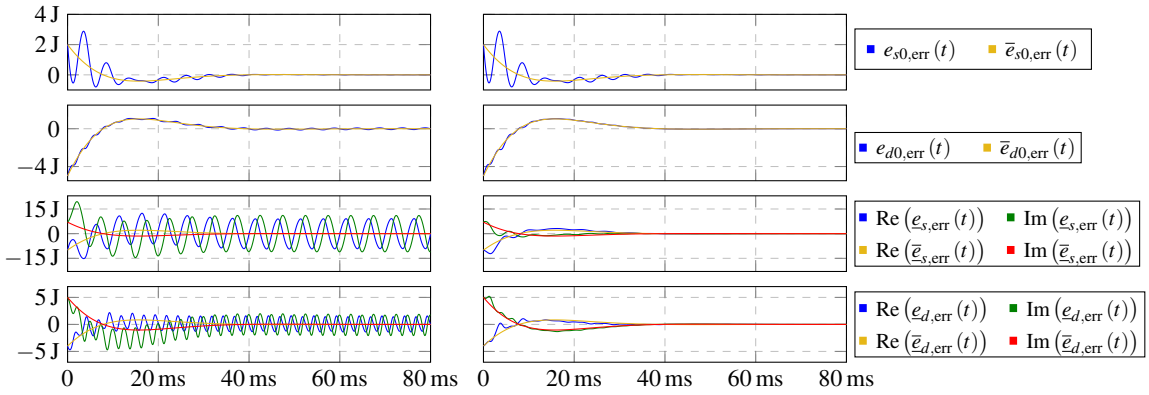

Fig. 5: Examples of error trajectory $t \mapsto \boldsymbol{e}_{\mathrm{err}}(t)$ of the proposed energy control system in Fig. 4 with the constant $\boldsymbol{E}$ (left column) and the stationary operating regime $\boldsymbol{e}_{\mathrm{rgm}}$ (right column) as the energy reference. The trajectory $t \mapsto \bar{\boldsymbol{e}}_{\mathrm{err}}(t)$ of the corresponding average system is determined by the designed error dynamics (16). The results are obtained by means of the simple choice (18), (19).

Measurement Results

For the implementation, the energy model in Fig. 4 is replaced by an MMC with current control and Pulse Width Modulation (PWM). The voltage of the dc-link capacitor is controlled to 600 V by an active grid side rectifier. The PWM frequency is 4884 Hz and the stator resistance of the PMSM is 0.59 Ω. During the test, the PMSM is free from any mechanical load, so its rotor is oriented by the stator currents.

The proposed controllers are tested with a step of the average value of the energy reference from an imbalanced to a balanced value at 0 ms. Fig. 6 shows the trajectories of (a) energy errors and (b) equivalent cell capacitor voltages for all six different variants indicated in the axis. In the simulations on the right, the energy error converges to zero whenever the regime $\boldsymbol{e}_{\mathrm{rgm}}$ is used as reference, while the errors do not vanish in case of the constant reference $\boldsymbol{E}$. These results coincide with the theoretical conclusions and show that the chosen value for the predetermined frequency ω_{cm} is large enough to ensure the stability of the proposed control system. The measurement of the energy error coincides well with the simulation, except for the small remaining errors in the measurement when the reference is given by the regime $\boldsymbol{e}_{\mathrm{rgm}}$. Fortunately, they do not result in a large mismatch between the measurement and the simulation of the cell capacitor voltage.

For a comprehensive comparison, some indexes reflecting the stationary and the transient performance are shown in Fig. 7: the peak-to-peak value $v_{C,\mathrm{pp}}$ of the equivalent cell capacitor voltages, the RMS value $I_{z,\mathrm{rms,sum}}$ of the arm currents for the stationary operation, and the Integral Time Absolute Error (ITAE) value $f_{\mathrm{ITAE}}(\boldsymbol{e}_z)$ of the difference between the arm energy $\boldsymbol{e}_z = \begin{pmatrix} e_{z1} & e_{z2} & e_{z3} & e_{z4} & e_{z5} & e_{z6} \end{pmatrix}^{\mathrm{T}}$ and its stationary solution. The results are plotted by varying controller parameter $k_{\mathrm{P,e}}$ and predetermined frequency ω_{cm} (settings see caption). The measured and simulated indexes are similar, except for $I_{z,\mathrm{rms,sum}}$ in Fig. 7b with the optimized controller, most likely because of an increased current control error due to the additional harmonics of higher order. The large reduction of $I_{z,\mathrm{rms,sum}}$ in the same figure is caused by the optimized controller and its objective function (20), which also reduces $v_{C,\mathrm{pp}}$, especially for the transient. Using the regime $\boldsymbol{e}_{\mathrm{rgm}}$ as reference systematically reduces $v_{C,\mathrm{pp}}$ and $I_{z,\mathrm{rms,sum}}$. However, the constant reference $\boldsymbol{E}$ is a noteworthy option, since it spares the costly regime determination. Compared with the common-mode voltage $v_{y0}^{\mathrm{1st+3rd}}$ (Fig. 3, red), the approximated trapezoidal wave v_{y0}^{trpz} (Fig. 3, blue) for the optimized controller leads to smaller $I_{z,\mathrm{rms,sum}}$ and $v_{C,\mathrm{pp}}$. On the whole, compared with the simple choice (18), (19), the optimization (18), (21) leads to a slight reduction of f_{ITAE}, except for the range $\omega_{\mathrm{cm}} > 2\pi \cdot 300\,\mathrm{rad/s}$. As expected, an increasing ω_{cm} leads to a smaller $v_{C,\mathrm{pp}}$. A larger controller parameter $k_{\mathrm{P,e}}$ decreases f_{ITAE} and $v_{C,\mathrm{pp}}$ during the transient, but increases $I_{z,\mathrm{rms,sum}}$ and $v_{C,\mathrm{pp}}$ slightly for the stationary operation.

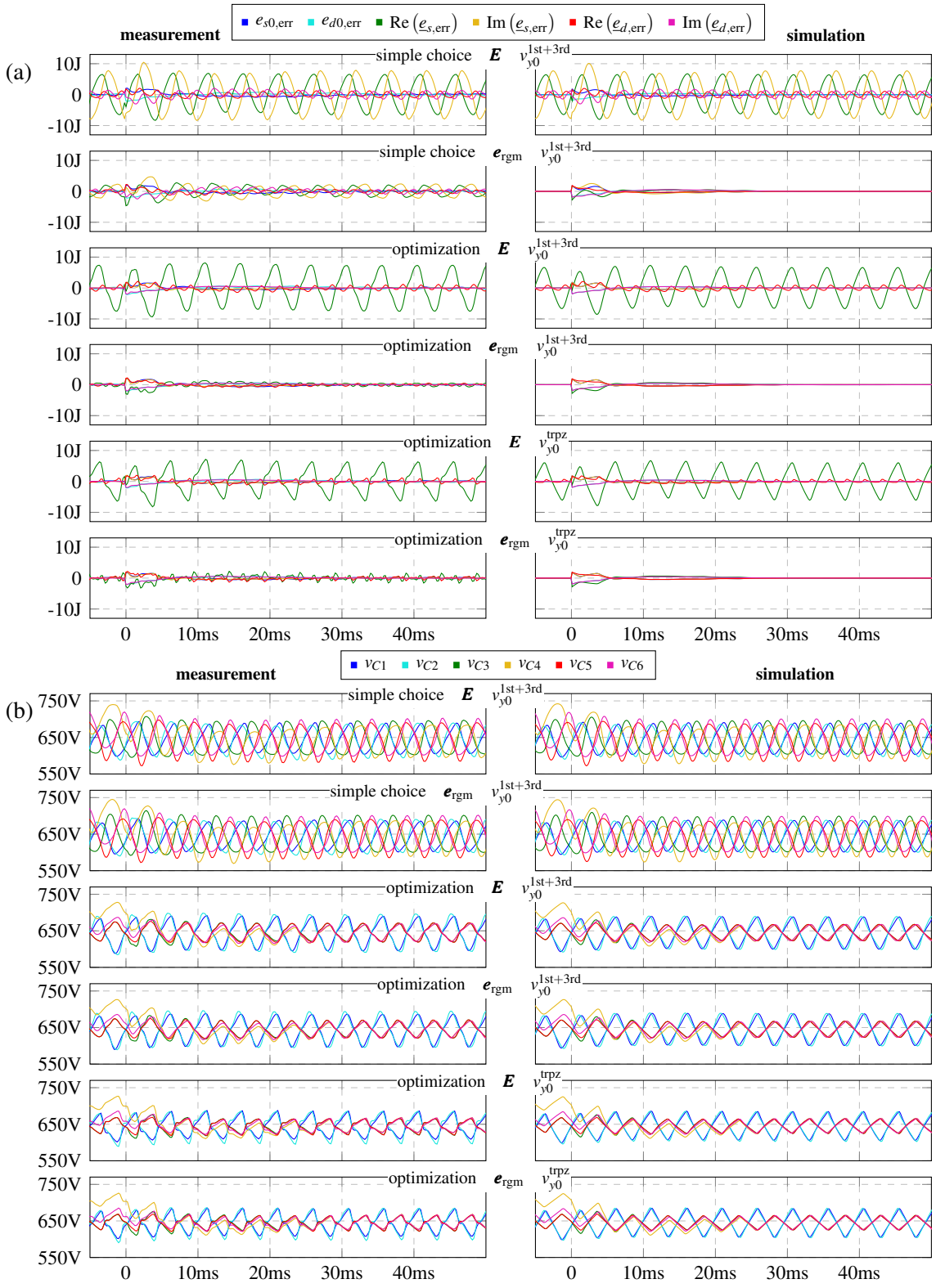

Fig. 6: Measurement and simulation results of the control system in Fig. 4: (a) energy errors (b) equivalent cell capacitor voltages. The average value of the energy reference steps at 0 ms, from an imbalanced value $(52\,\mathrm{J}, -2\,\mathrm{J}, -3\,\mathrm{J}, 2\,\mathrm{J}, 2\,\mathrm{J}, -2\,\mathrm{J})$ to a balanced value $(50\,\mathrm{J}, 0, 0, 0, 0, 0)$. Settings: $\omega_{\mathrm{cm}} = 203.5\,\mathrm{rad/s}$, $k_{\mathrm{P,e}} = 250\,\mathrm{Hz}$, $k_{\mathrm{I,e}} = k_{\mathrm{P,e}}^2/2$, $\underline{i} = \underline{I}^{[0]} = 5\,\mathrm{A}$.

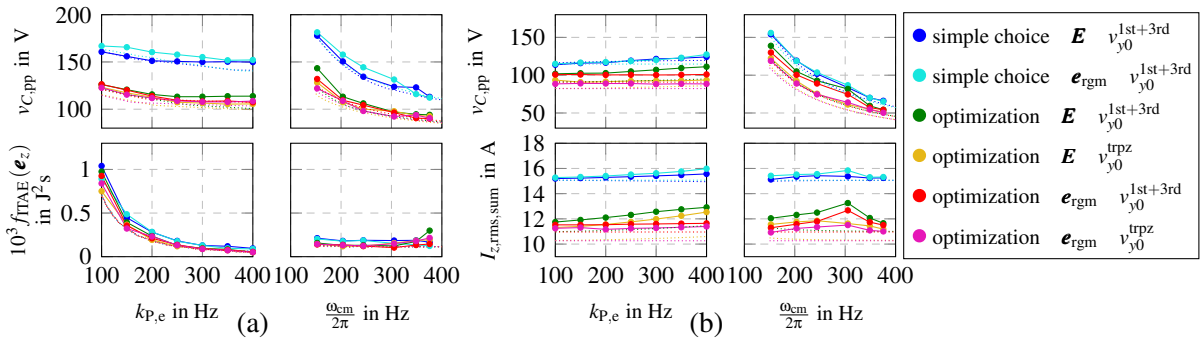

Fig. 7: Measurements (solid) and simulations (dotted) of the indexes reflecting (a) the transient and (b) the stationary performance of the proposed energy control system. Settings: $\omega_{\mathrm{cm}} = 203.5\,\mathrm{rad/s}$ for the 1st and 3rd column, $k_{\mathrm{P,e}} = 250\,\mathrm{Hz}$ for the 2nd and 4th column, $k_{\mathrm{I,e}} = k_{\mathrm{P,e}}^2/2$, $\underline{i} = \underline{I}^{[0]} = 5\,\mathrm{A}$.

Conclusion

A new controller design framework for periodic systems is presented relying on the results in [11]. It is applied to the energy controller design of MMCs feeding a PMSM at standstill. This provides a rigorous stability analysis for the proposed energy control system, that is, an exponential convergence of the energy error in case of the calculated stationary operating regime $\boldsymbol{e}_{\mathrm{rgm}}$ as the reference (this coincides with the more common approaches like in [5]), and a global stability in case of the constant energy references (this coincides with the less common approaches like in [1]). These theoretical conclusions are confirmed by simulations and measurements. Besides the controller with the simple choice, an optimized controller is derived by quadratic programming. The validity of the constant energy reference and the improved performance of the optimization w.r.t. the peak-to-peak value of the cell capacitor voltages and the arm current RMS is verified by measurement results.

References

[1] R. Lizana, et al. Control of arm capacitor voltages in modular multilevel converters. IEEE Trans. Power Electron., 31(2):1774–1784, 2016.

[2] H. Fehr, et al. Eigenvalue optimization of the energy-balancing feedback for modular multilevel converters. IEEE Trans. Power Electron., 34(11):11482–11495, 2019.

[3] A. Gensior, et al. Modeling and energy balancing control of modular multilevel converters using perturbation theory for quasi-periodic systems. IEEE Trans. Power Electron., 36(2):2201–2217, 2021.

[4] H. Bärnklau, et al. A model-based control scheme for modular multilevel converters. IEEE Trans. Ind. Electron., 60(12):5359–5375, 2013.

[5] J. Kolb, et al. Cascaded control system of the modular multilevel converter for feeding variable-speed drives. IEEE Trans. Power Electron., 30(1):349–357, 2015.

[6] A. E. Leon, et al. Energy balancing improvement of modular multilevel converters under unbalanced grid conditions. IEEE Trans. Power Electron., 32(8):6628–6637, 2017.

[7] M. Espinoza, et al. Modelling and control of the modular multilevel converter in back to back configuration for high power induction machine drives. In IECON 2016, pages 5046–5051, 2016.

[8] Ö. C. Sakinci, et al. Generalized dynamic phasor modeling of the mmc for small-signal stability analysis. IEEE Trans. Power Del., 34(3):991–1000, 2019.

[9] Y. Ma, et al. Stability analysis of modular multilevel converter based on harmonic state-space theory. IET Power Electronics, 12(15):3987–3997, 2019.

[10] F. Verhulst. Nonlinear Differential Equations and Dynamical Systems. Springer, 2000.

[11] H. K. Khalil. Nonlinear systems. Prentice Hall, Upper Saddle River, NJ, 3. ed. edition, 2002.

[12] M. Hagiwara, et al. Start-up and low-speed operation of an electric motor driven by a modular multilevel cascade inverter. IEEE Trans. Ind. Appl., 49(4):1556–1565, 2013.

[13] D. Graham, et al. The synthesis of ”optimum” transient response: Criteria and standard forms. Transactions of the American Institute of Electrical Engineers, Part II: Applications and Industry, 72(5):273–288, 1953.

[14] Q. Gui, et al. Energy-balancing of a modular multilevel converter using an online trajectory planning algorithm. In EPE’20 ECCE Europe, 2020.

[15] Q. Gui, et al. Energy-balancing of a modular multilevel converter with pulsed dc load using an online trajectory planning algorithm. In EPE’21 ECCE Europe, 2021.